HELDA
HELSINGIN YLIOPISTO
HELSINGFORS UNIVERSITET
UNIVERSITY OF HELSINKI

UNIVERSITY OF HELSINKI

https://helda.helsinki.fi

Characterization of magnetic Czochralski silicon devices with aluminium oxide field insulator : effect of oxygen precursor on electrical properties and radiation hardness

Ott, J.

2021-05

Ott , J , Bharthuar , S , Gädda , A , Arsenovich , T , Bezak , M , Brücken , E , Golovleva , M , Härkönen , J , Kalliokoski , M , Karadzhinova-Ferrer , A , Kirschenmann , S , Litichevskyi , V , Luukka , P , Martikainen , L & Naaranoja , T 2021 , ' Characterization of magnetic Czochralski silicon devices with aluminium oxide field insulator : effect of oxygen precursor on electrical properties and radiation hardness ' , Journal of Instrumentation , vol. 16 , no. 5 , P05011 . https://doi.org/10.1088/1748-0221/16/05/P05011

http://hdl.handle.net/10138/343197
https://doi.org/10.1088/1748-0221/16/05/P05011

acceptedVersion

Downloaded from Helda, University of Helsinki institutional repository.

This is an electronic reprint of the original article.

This reprint may differ from the original in pagination and typographic detail.

Please cite the original version.

Prepared for submission to JINST

Characterization of magnetic Czochralski silicon devices with aluminium oxide field insulator: effect of oxygen precursor on electrical properties and radiation hardness

J. Ott,[a,b,1] **S. Bharthuar**[a] **A. Gädda**[a,c] **T. Arsenovich**[a] **M. Bezak**[a,d] **E. Brücken**[a] **M. Golovleva**[a,d] **J. Härkönen**[a,e] **M. Kalliokoski**[a,e] **A. Karadzhinova-Ferrer**[e] **S. Kirschenmann**[a] **V. Litichevskyi**[a,f] **P. Luukka**[a,d] **L. Martikainen**[a] **T. Naaranoja**[a]

[a] *Helsinki Institute of Physics, Gustaf Hällströmin katu 2, FI-00014 University of Helsinki, Finland*
[b] *Aalto University, Department of Electronics and Nanoengineering, Tietotie 3, FI-02150 Espoo, Finland*
[c] *Advacam Oy, Tietotie 3 (P.O. Box 1000), FI-02044 VTT, Finland*
[d] *Lappeenranta University of Technology, Skinnarilankatu 34, FI-53850 Lappeenranta, Finland*
[e] *Ruđer Bošković Institute, Bijenička cesta 54, HR-10000 Zagreb, Croatia*
[f] *Specom Oy, Tekniikantie 2A 326, FI-02150 Espoo, Finland*

E-mail: jennifer.ott@helsinki.fi

Abstract:

Aluminium oxide (Al_2O_3) has been proposed as an alternative to thermal silicon dioxide (SiO_2) as field insulator and surface passivation for silicon detectors, where it could substitute p-stop/p-spray insulation implants between pixels due to its negative oxide charge, and enable capacitive coupling of segments by means of its higher dielectric constant. Al_2O_3 is commonly grown by atomic layer deposition (ALD), which allows the deposition of thin layers with excellent precision.

In this work, we report the electrical characterization of single pad detectors (diodes) and MOS capacitors fabricated on magnetic Czochralski silicon substrates and using Al_2O_3 as field insulator. Devices are studied by capacitance-voltage, current-voltage, and transient current technique measurements. We evaluate the influence of the oxygen precursors in the ALD process, as well as the effect of gamma irradiation, on the properties of these devices. We observe that leakage currents in diodes before the onset of breakdown are low for all studied ALD processes. Charge collection as measured by transient current technique (TCT) is also independent of the choice of oxygen precursor. The Al_2O_3 films deposited with O_3 possess a higher negative oxide charge than films deposited by H_2O, However, in diodes a higher oxide charge is linked to earlier breakdown, as has been predicted by simulation studies. A combination of H_2O and O_3 precursors results in a good compromise between the beneficial properties provided by the respective individual precursors.

Keywords: Czochralski Silicon; Atomic Layer Deposition; Aluminium Oxide; Radiaton Damage

[1] Corresponding author.

Contents

1 Introduction **1**

2 Sample Fabrication and Characterization **2**
2.1 Detector processing 2
2.2 Characterization 3

3 Results and discussion **6**
3.1 Impact of ALD oxidant 6
3.2 Effects of gamma irradiation 10

4 Summary and conclusions **18**

1 # 1 Introduction

2 Silicon detectors are used in high-energy physics experiments as vertexing and tracking detectors.
3 In the detector upgrades for the high-luminosity stage of the Large Hadron Collider, foreseen for
4 2027, the radiation levels at the innermost silicon layers of the experiments' tracking detectors will
5 increase to > 2×10^{16} n_{eq}cm^{-2}, and 12 MGy, e.g. in the CMS Tracker detector.[1]
6 To benefit from the higher mobility of electrons compared to the holes in Si, modern detectors
7 are realized with segmented n^+ implants, on a p-type substrate. In this sensor design, the weak
8 positive oxide charge of the traditionally used dielectric in pixel detectors, silicon dioxide (SiO_2),
9 obtained by thermal oxidation, would lead to a loss of spatial resolution, as the electron-collecting
10 segments are effectively connected to each other.[2, 3] This is usually avoided by additional p-
11 type implant between the segments, referred to as p-spray or p-stop, depending on its width
12 and concentration. However, p-spray/p-stop implants require additional implantation and high-
13 temperature process steps, as well as more space on the detector.[4, 5]
14 As an alternative to the combination of SiO_2 and insulation p^+ implants by an oxide with
15 negative charge, aluminium oxide (Al_2O_3) has been proposed.[6–8] Al_2O_3 is widely used as surface
16 passivation layer in the silicon photovoltaics industry.[9] The excellent surface passivation achieved
17 with Al_2O_3 includes contribution from both chemical passivation by termination of dangling bonds
18 on the Si surface, and field-effect passivation due to its high negative oxide charge, which repels
19 electrons and therefore prevents them from recombining at remaining interface and near-interface
20 defects.[10, 11]
21 One established way to fabricate Al_2O_3 thin films is by atomic layer deposition (ALD), which
22 allows the uniform, conformal and precisely controlled deposition of thin films by separated and
23 self-terminating gas-solid reactions of typically two gaseous precursors separated by a purge of
24 inert gas.[12–14]

A critical factor for the properties of Al_2O_3 thin films is the oxygen source used in film deposition, also referred to as the oxidant. Earlier studies have reported that Al_2O_3 films deposited with ozone (O_3) instead of water have higher negative charge and provide better surface passivation than films deposited with water.[15, 16] The best performance was achieved when a combination of water and ozone was used.[16, 17] Therefore, we study the impact of the oxidant on electrical properties of high-resistivity silicon devices using aluminium oxide, with Al_2O_3 deposited by water, ozone, or a combination hereof.

Due to the potentially better radiation hardness of Czochralski silicon compared to standard float zone silicon, the following experiment series was conducted on high-resistivity p-type magnetic Czochralski silicon.[18, 19]

2 Sample Fabrication and Characterization

2.1 Detector processing

Detector fabrication was carried out in the cleanroom facilities of Micronova Nanofabrication Centre. The process was implemented on 6-inch Magnetic Czochralski silicon wafers from Okmetic Oy, with a thickness of 320 µm and crystal orientation <100>. The wafers were boron-doped to a resistivity specified as 4-8 kΩcm.

The processing steps are summarized below. Lithography was carried out by standard techniques including priming, resist development, baking, and resist stripping. Photoresist patterning was performed with a mask aligner in soft-contact mode.

First, wafers underwent wet oxidation at 1000°C in order to obtain an approximately 300 nm thick thermal oxide as hard mask for ion implantation. The oxidation was preceded by standard chemical cleaning sequence (RCA cleaning).[20] Alignment marks were etched by reactive ion etching (RIE), using CHF_3 and SF_6 ions to etch SiO_2 and Si, respectively. For ion implantation, the SiO_2 on the wafer front surface was patterned by wet etching with a buffered hydrofluoric acid (BHF) etchant solution at 30°C. The oxide on the back surface was removed completely. Ion implantation was carried out in an Eaton 8200 Ion implanter, implanting the front side with 60 keV phosphorous ions and the back side with 20 keV boron ions, both to target total doses of $1\times10^{15}\,cm^{-2}$. After implantation, the mask oxide was etched away with BHF, the wafers were RCA-cleaned, and subjected to a 46 min anneal at 1100°C in dry oxidation conditions, in order to diffuse the implanted ions deeper into the bulk. The resulting fresh thermal SiO_2 was again removed with BHF, and RCA cleaning was repeated. This was followed by the deposition and patterning of Al_2O_3 as dielectric.

Al_2O_3 was deposited at 200°C in a Beneq TFS-500 batch-type ALD reactor, using $Al(CH_3)_3$ (trimethyl aluminium, TMA) as the metal precursor. One ALD cycle consisted of a 400 ms TMA pulse, followed by a 7 s N_2 purge, the oxidant pulse and finally another 7 s N_2 purge. For the films deposited only using water, the H_2O pulse was 500 ms; in the case of ozone, the O_3 pulse was set to 7 s; finally for the combined oxidants, the sequence was formed by a 500 ms H_2O and 7 s O_3 pulse. Each deposition consisted of 700 cycles. Since the growth rate differed slightly for the different oxidants, this resulted in film thicknesses of 75.3 nm, 72.3 nm and 84.1 nm for H_2O, O_3, and H_2O + O_3, respectively.

Etching of the Al_2O_3 films was done with a commercial Honeywell PWS 80-16-4 phosphoric acid etchant at 50°C. Etch rates for metallic Al and Al_2O_3 in this solution are sufficiently different for the chemical to also be used later in the process for patterning of the Al metallization layer without significant damage to the Al_2O_3. For the metal contacts, aluminium was deposited by direct current (DC) sputtering and patterned with a commercial H_3PO_4-HNO_3 Al etchant at 50°C. Finally, wafers were sintered for 30 min at 370°C in order to establish the negative oxide charge in Al_2O_3. This simultaneously served as sintering step for the Al metallization. Figure 1 shows a photograph of a final wafer before dicing.

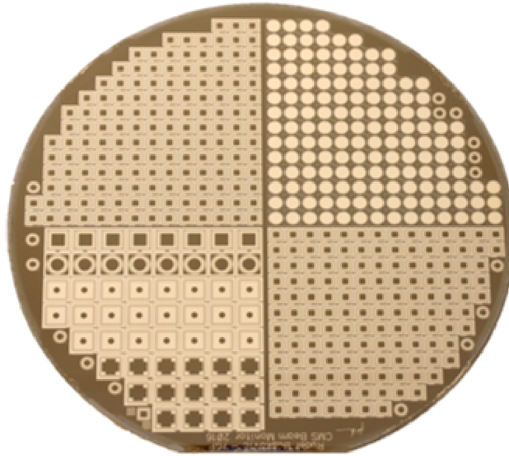

Figure 1: Photograph of a full 6-inch wafer before dicing.

2.2 Characterization

The wafer layout consisted of different diodes and MOS capacitors, arranged according to wafer quarters:

- 5×5 mm^2 square diodes.
- 5×5 mm^2 square diodes with almost fully metallized central pad and only small optical opening.
- 2.5×2.5 mm^2 small square diodes.
- Large round diodes with a diameter of 5 mm.
- MOS capacitors with diameter of 4 mm.

All diodes feature a broader innermost guard ring, and a series of 16 narrower outer guard rings, for electric field termination around the central pad.
The results presented in the following chapter were obtained from the large round and square diodes with wide optical openings (shown in Figure 2), as well as the MOS capacitors. Schematic cross-sections of these devices are shown in Figure 3.

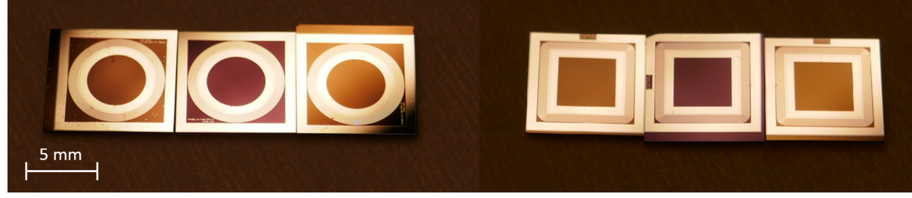

Figure 2: Photographs of large round and large square diodes.

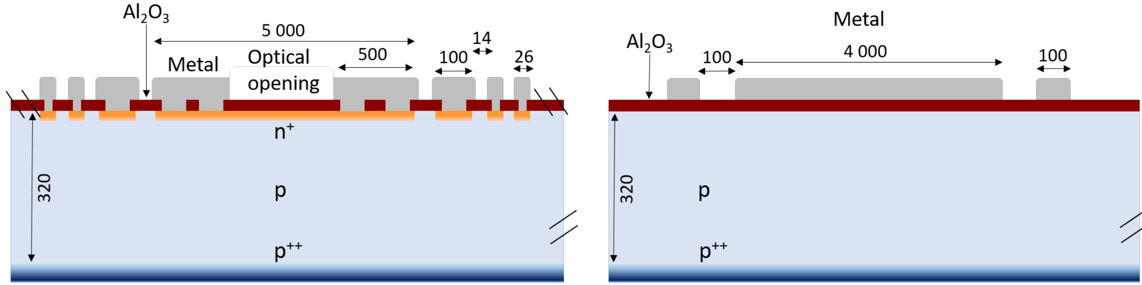

Figure 3: Schematic cross-sectional view of diodes (left) and MOS capacitors (right) characterized in this study. All dimensions are in µm.

Leakage current densities, depletion voltage, and silicon bulk capacitance after full depletion were determined by current-voltage (I-V) and capacitance-voltage (C-V) measurements on pad diodes.

The effective doping concentration N_{eff} is determined from the full depletion voltage V_{fd}, using the permittivities of the vacuum and silicon, as well as the substrate thickness D:

$$N_{eff} = \frac{2\epsilon_0 \epsilon_{Si} V_{fd}}{qD^2} \tag{2.1}$$

The substrate resistivity ρ can be calculated from effective doping concentration, using the charge carrier mobility, which in a p-type substrate is the hole mobility μ_h:

$$\rho = \frac{1}{q\mu_h N_{eff}} \tag{2.2}$$

Based on C-V measurement data, the full depletion voltage in a sensor is defined as the voltage after which the capacitance remains constant. In practice, this is set as the the center point of the "knee" of the $1/C^2$-V curve, or as 99% of the maximal capacitance.

C-V measurements on MOS capacitors are used to determine the effective oxide charge, as well as an estimation of mobile charges, of Al_2O_3.[21] The capacitance of a MOS capacitor responds to variations in voltage applied from the metal contact over the oxide, known as the gate. For a p-type substrate, negative voltage attracts charge carriers to the gate in a state of accumulation, where the capacitance is at its maximum and is determined only by the oxide layer. Upon reduction of the voltage and further sweep to positive gate voltages, band bending reaches the flat-band condition and the system is eventually driven into inversion. At low frequencies, the minority carriers (here in a p-type substrate, electrons) form an inversion charge layer at the oxide-silicon interface, which

increases the capacitance after depletion again to a maximum value with positive bias voltage. However, at high frequencies, the minority carriers cannot follow the sweep rate of the probing AC voltage. Therefore, further increase of the bias voltage towards the inversion condition registers additional capacitance from the space-charge region below the oxide, and the total capacitance of the silicon and oxide in series is thus very small. This results in a typical S-shaped curve for high-frequency MOS capacitor C-V measurements, with the center (inflection point) indicating the flat-band voltage V_{fb}. From the C-V curve, V_{fb} and oxide capacitance C_{ox} can be extracted as the voltage at the inflection point and the overall maximum capacitance, respectively.

Assuming an overall charge-neutral system, the oxide charge Q_{eff} can be determined from V_{fb} according to Equation 2.3, where ΔV_{fb} refers to the difference of the measured flatband voltage to an ideal case with no oxide charge, where consequently V_{fb} would be zero.

$$Q_{eff} = -C_{ox}\Delta V_{fb} \tag{2.3}$$

I-V and C-V measurements were performed in a Karl Suess probe station. For I-V measurements, a Keithley 2410-C SourceMeter unit was used to supply the bias voltage through the probe station chuck to the backplane of the device, and simultaneously to measure the total current. In diodes, the main guard ring was grounded through a probe needle, and pad currents were read separately with a Keithley 6487 PicoAmmeter connected through a probe needle to the device's central metal pad. For C-V, the device was connected by probe needle through a current-potential decoupling box to an Agilent E4980A Precision LCR meter, with the Keithley 2410-C still supplying the DC bias voltages. Capacitances were recorded at an AC frequency of 1 kHz, unless otherwise mentioned. Due to the technical limitations of this setup, only high-frequency C-V curves for MOS capacitors were obtained.

Transient current techniques (TCT) enable the extraction of various semiconductor properties, including charge collection, depletion voltage, electrical field profile, trapping time and effective dopant concentration.[22–25] Figure 4 illustrates the contribution of charge carriers to the signal for different lasers used in TCT.

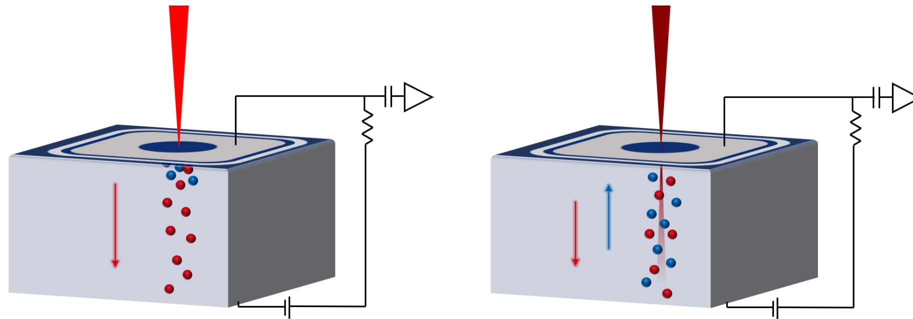

Figure 4: Schematic representation of charge carrier generation in TCT with red (left) and IR laser (right).

In TCT measurements with a red laser, a cloud of electron-hole pairs is created only within a few µm from the surface of the sensor facing the radiation source. In the electric field over the sensor, the charge carriers drift towards the respective electrodes. One of the charge carrier types,

either electrons or holes depending on the device structure, is immediately collected by the entrance surface electrode - as the RC time constant of the preamplifier is usually much larger than the drift time of these charge carriers, they are only seen in the sharp rise of the signal, but do not contribute to the transient. Carriers of the other type traverse through the entire bulk, and the resulting transient current signal, induced by charge moving in an electrical field according to the Shockley-Ramo theorem, is detected by an oscilloscope.[26, 27] The shape of this signal is directly proportional to the electric field inside the sensor, as well as the weighting field, which in the present case of parallel electrodes is constant.

The absorption of light from an infrared laser, on the other hand, occurs over several hundreds of µm, generating electron-hole pairs throughout the thickness of the silicon sensor. The signal generated in this way is a sum of both types of charge carriers, and provides a better approximation of the interaction of a high-energy charged particle with the detector. The charge collection efficiency (CCE) of a sensor can be determined by integrating the waveforms obtained with the IR laser, which corresponds to the charge of the electron-hole pairs generated by excitation with the laser. Saturation of the collected charge in non-irradiated sensors, or sensors after low irradiation doses, can be interpreted as the onset of full depletion.

In this report, optical excitation for TCT was performed with a PicoQuant PDL 800-B picosecond pulsed diode laser connected via an optical fiber and focusing optics to red (λ = 660 nm) or IR (λ = 1064 nm) laser heads, at a rate of 2.5 MHz. The intensity of an individual laser pulse corresponded to the charge generated by 2-8 and 5-9 minimum ionizing particles (MIPs), respectively. The laser illumination was directed to the optical openings on the sensor front plane. Here, the studied sensors were n-in-p diodes, so the red-laser TCT signal displays holes drifting through the device, while the electrons are immediately collected away by the front contact. The sensor was connected to the readout, through a Picosecond 5531 HV bias-T, with a probehead needle placed onto the front side pad metallization, while the bias voltage was supplied to the backplane through the metal plating on a printed circuit board by a Keithley 2410 SourceMeter with an additional Particulars HV filter. The DC reading of the bias voltage supply was monitored during the measurements. The transient signals were obtained with a Particulars 53 dB broadband RF amplifier (10kHz-2GHz) and a LeCroy WavePro 7300A 3 GHz analog bandwidth fast oscilloscope as averages over 300 waveforms. An offset correction for the onset time and baseline was applied to all measurements.

3 Results and discussion

3.1 Impact of ALD oxidant

Figure 5 shows examples of pad and total currents for diodes with Al_2O_3 films grown using different oxidants. All leakage currents are low, with 4-6 nA/cm^2 at -150 V (Figure 5a). The total currents, i.e. including contributions through the guard ring, are higher, and show that breakdown occurs through the periphery of the device and not through the bulk at the central pad. A wide spread in breakdown voltage of over 40 V is observed even in devices from the same wafers, which is at least in part attributed to storage in ambient air without moisture or temperature control. The average breakdown voltage correlates clearly with the ALD oxidant: films deposited with ozone exhibit breakdown much earlier, even just above full depletion, than films deposited with water (Figure 5b). Although a higher oxide charge, here provided by the O_3 oxidant, is favorable for

174 efficient inter-segment insulation, it predisposes the device for early breakdown at the guard ring:
175 depending on the oxide charge and also the dimensions of the device, the electric field between the
176 segments may become high enough (at peak values of ca. 200 kV/cm) to lead to carrier avalanches
177 and breakdown between the guard rings.[28] This should be taken into account in device design
178 and fabrication, such as the width and distance of the guard rings, in relation to the oxide charge
179 obtained with a specific Al_2O_3 deposition process.

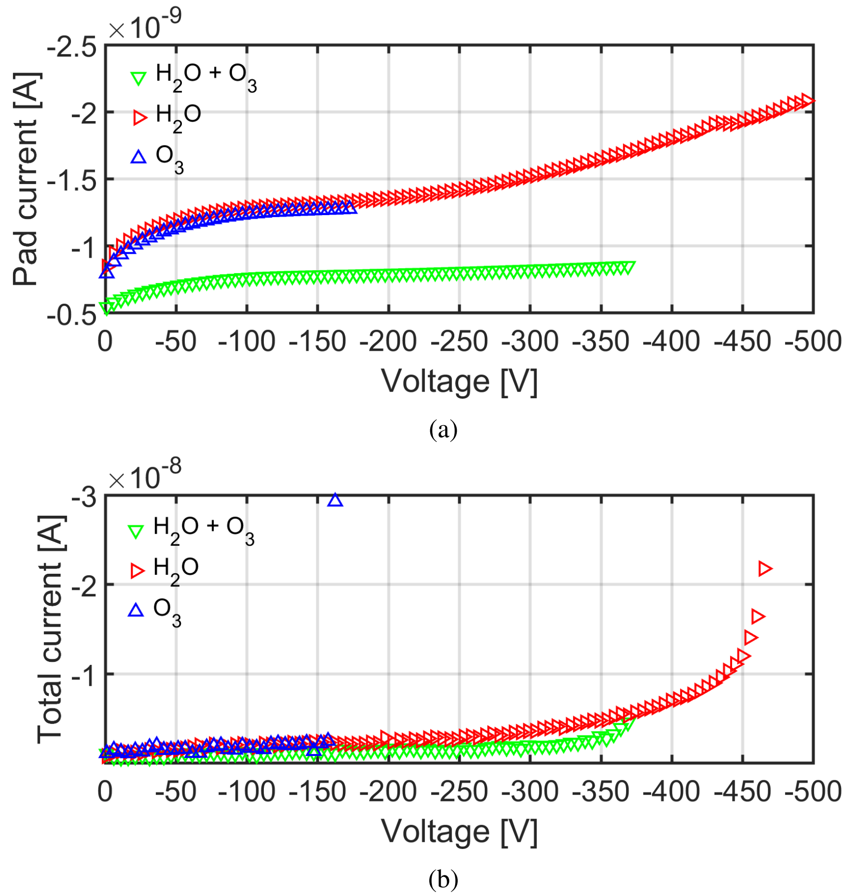

Figure 5: a) Leakage currents measured from the central pad, and b) total leakage currentsover the entire device including the main guard ring, for large round test structure diodes with Al_2O_3 films grown using different oxidants.

180 An example of a diode C-V curve is shown in Figure 6. It indicates full depletion (defined as
181 the point where capacitance remains constant) between around -120 and -140 V. From $1/C^2$ (cf.
182 Figure 11a) the full depletion voltage is extracted as -132 V. This corresponds to an effective doping
183 concentration of 1.7×10^{12} cm^{-3} and a resistivity of 8.3 kΩcm, which is slightly higher than the
184 original wafer specifications. A potential reason for this deviation is discussed below in context of
185 gamma irradiation and the observed resistivity of pixel detector wafers.

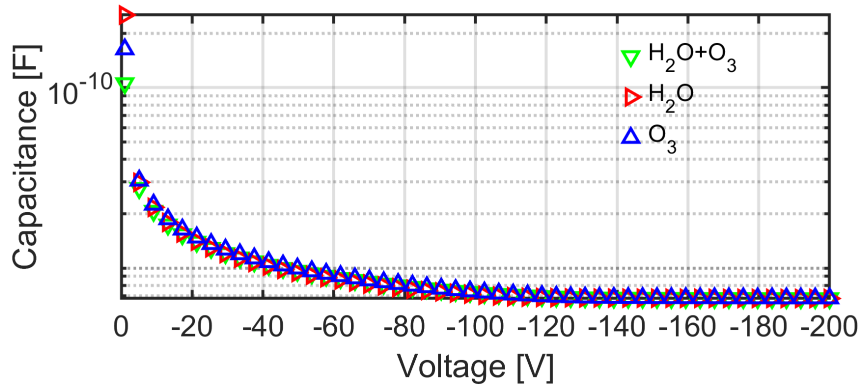

Figure 6: C-V curve of large round diodes with Al_2O_3 films deposited with different oxidants.

Diodes were further studied by laser TCT with red and infrared lasers. The signals were obtained as an average over 300 waveforms at each step of 10 V. The evolution of the TCT signal with bias voltage is shown in Figure 7. The ALD oxidant does not have an effect on these measurements, as could be expected, since the signal is caused by the drift of charge carriers through the bulk of the detector to the collecting electrodes, which are in direct contact with the implants and thus not affected by the dielectric. An edge at the lower end of the electric field, indicating full depletion of the device, appears around -130 V, which is in good agreement with C-V measurements. Even after full depletion, the decrease in signal duration with bias voltage, due to proportional increase in drift velocity with electric field, is apparent.

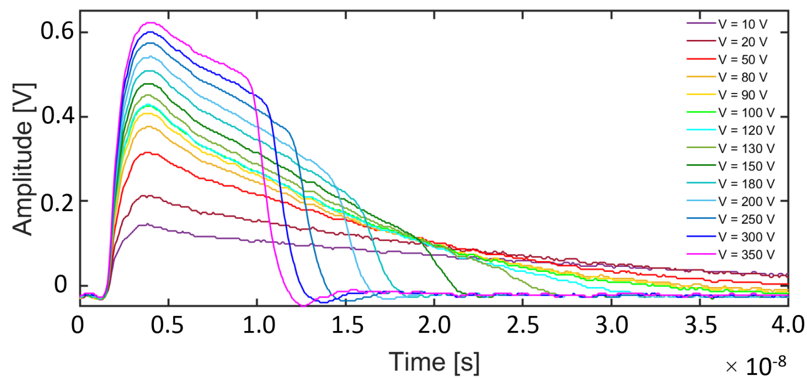

Figure 7: Transient signal generated with red laser for a representative large round diode. Signal duration at 150 V is around 20 ns.

MOS capacitor C-V curves for each oxidant are compared in Figure 8. Curves were recorded both from accumulation of the gate towards inversion, i.e, in this case for p-type substrate, starting from negative gate voltages or zero, and vice-versa. The small differences in oxide capacitances are explained by the slightly different film thicknesses.

All films exhibit a positive flatband voltage and therefore a negative oxide charge, which is however clearly lower for the film deposited with H_2O compared to the nearly identical charge of

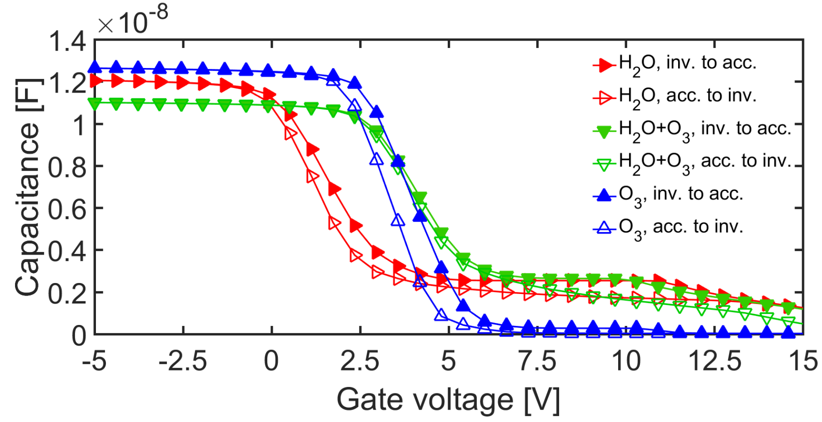

Figure 8: MOS capacitor CV curves for Al_2O_3 films deposited with different oxidants.

201 films deposited with O_3 and $H_2O + O_3$. The numeric comparison is shown in Table 1.
202 In lack of low-frequency C-V curves, no interface defect density (D_{it}) values could be reliably
203 extracted in this way. When examining the slope of the measured C-V curve as an indication
204 of interface quality, differences between interface defect densities for the different oxidants appear
205 negligible. However, the hysteresis of the curves, i.e. the gap between measurements from inversion
206 to accumulation and vice versa, can be interpreted as mobile interface charge, with values also shown
207 in Table 1.

Table 1: Electrical properties of diodes and MOS capacitors fabricated with Al_2O_3 using different ALD oxidants.

Oxidant species	**H_2O**	**O_3**	**$H_2O + O_3$**
Leakage current at -150 V [nA]	1.3	1.2	0.8
Breakdown voltage [V]	450	150	350
Oxide charge Q_{eff} [$\times 10^{12}$ qcm^{-2}]	-1.09	-2.22	-2.92
Mobile interface charge (Q_{eff} hysteresis) Q_m [$\times 10^{11}$ qcm^{-2}]	2.52	4.09	3.50

208 ### 3.2 Effects of gamma irradiation

209 A set of diodes and MOS capacitors were irradiated with gamma radiation from a Co-60 source at
210 the Radiation Chemistry and Dosimetry Laboratory at Ruđer Bošković Institute in Zagreb, Croatia.

211 For comparison, some data of corresponding diode and MOS capacitor devices from a pixel
212 detector wafer (fabrication described in [29]) is included. The key differences of the latter to the
213 fabrication process described in this article are the additional bias resistor and surface passivation
214 layers, which do not directly affect the functionality of diodes and MOS capacitor structures. The
215 larger surface area of the devices on the pixel detector wafer is accounted for in the results by scaling
216 the relevant quantities by area. Irradiations were conducted at different times and total doses for
217 devices from test structure and pixel detector wafers.

218 Figure 9 shows the evolution of bulk leakage currents in diodes with gamma radiation dose.
219 It is notable that the breakdown voltage is increased to > 500 V for all ALD oxidants, effectively
220 eliminating the major disadvantage of the O_3 -based processes, especially O_3 only. In contrast,
221 irregular high leakage currents are observed for the diodes with a H_2O -based Al_2O_3 film. This may
222 be caused, or contributed to, by the large blisters reported in ref.[30](incl. Supporting Information)
223 for thick Al_2O_3 films on high-resistivity silicon substrates. At a blistering site, the Al_2O_3 film
224 is delaminated from the Si substrate or removed completely, and may thus not provide sufficient
225 insulation against the higher radiation-induced leakage currents. A closer inspection excluding the
226 samples in fabricated with H_2O as oxidant is shown in Figure 10.

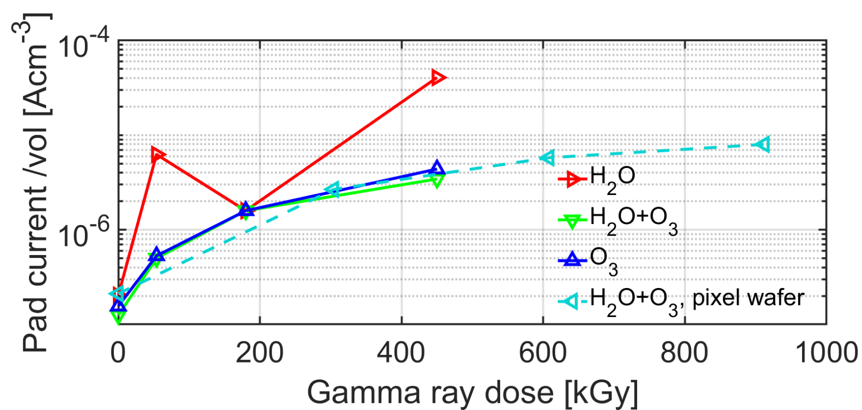

Figure 9: Pad (bulk) leakage current in gamma-irradiated diodes for different oxidants.

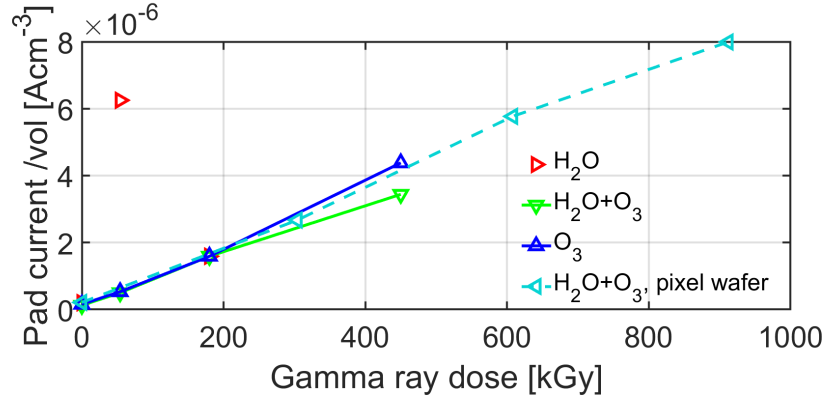

Figure 10: Pad (bulk) leakage current in gamma-irradiated diodes, closer comparison between O_3 and $H_2O + O_3$ processes.

227 A linear increase of leakage current with gamma radiation dose, which is characteristic for
228 n-type oxygenated float zone or Cz silicon as opposed to nonlinear behavior for silicon substrates
229 with low oxygen concentration[31, 32], is also observed here in the p-type MCz substrate. Taking
230 into account only diodes fabricated with O_3 and $H_2O + O_3$ ALD processes in Fig. 10, the increase of
231 leakage current, described by the α parameter, is very similar for the two different batches and across
232 wafers in the test structure process, confirming similar initial substrate and film quality, and reliability
233 of irradiations. The average value of 2.60×10^{-10} A cm^{-2} kGy^{-1} or 8.95×10^{-9} A cm^{-3} kGy^{-1},
234 respectively, is of the same order of magnitude as literature values for n-type silicon with high
235 oxygen concentrations, with 1×10^{-10} A cm^{-2} kGy^{-1}[33] or $> 5 \times 10^{-9}$ A cm^{-3} kGy^{-1}[31, 32].
236 No other reported alpha parameter values for p-type MCz silicon were found. Figure 11 shows
237 the change of full depletion voltage with gamma radiation dose for test structure and pixel detector
238 wafer diodes. In the test structure diodes (Fig. 11a), a decrease in V_{fd} with dose is observed,
239 whereas in the pixel detector diodes (Fig. 11b), V_{fd} first decreases and then increases again.

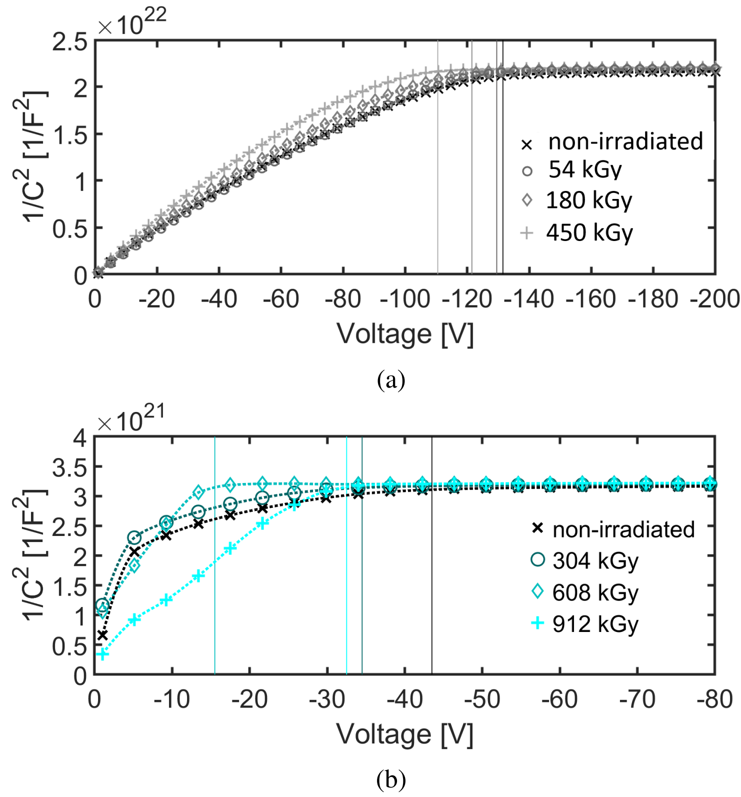

Figure 11: Change of C-V characteristics, prominently a shift of full depletion voltage, with gamma irradiation in diodes from a) test structure wafers for any oxidant, b) pixel detector layout with Al_2O_3 deposited with H_2O + O_3 oxidants.

240 When converting V_{fd} into effective doping concentration (Fig. 12), it appears that compensation
241 (or deactivation) of the p-type doping occurs. For the pixel detector diodes, this soon leads to space
242 charge sign inversion (SCSI) due to their lower initial bulk doping.

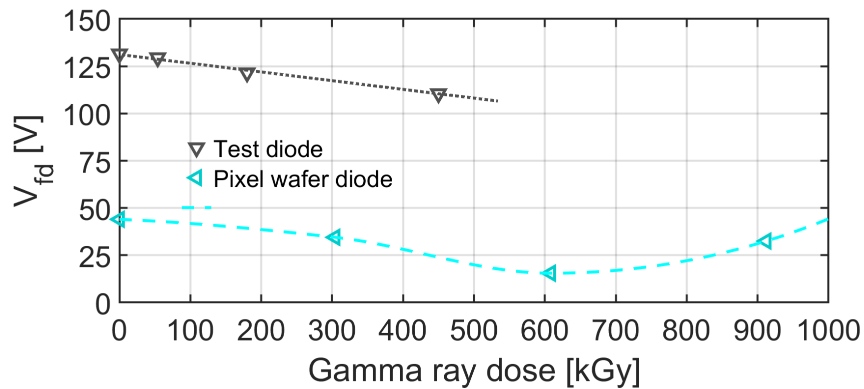

Figure 12: Change of full depletion voltage and thus compensation of negative space charge with gamma irradiation in diodes. Lower initial doping concentration and space charge sign inversion is visible for newer pixel detector layout diodes.

It is known that gamma irradiation causes the formation of positive space charge in oxygen-rich material[31, 33], which can consequently lead to space charge compensation and eventually sign inversion in p-type MCz silicon[34]. With an effective doping concentration of 6.3×10^{11} cm^{-3} and a resistivity of 22 kΩcm, the bulk doping after processing for pixel detector wafers was already much lower than the original wafer specifications. Such a difference may be due to a deviation of substrate properties in the manufacturing process, for example a change in oxygen concentration across the silicon ingot. Alternatively, this could be an indication that thermal donors were unintentionally introduced into the MCz substrate over the detector fabrication process. To achieve lower effective doping concentrations and thus lower depletion voltages, thermal donors in Cz-Si have been used even intentionally. [35, 36] Although even the test structure wafers have an initial resistivity of 8.3 kΩcm as calculated from C-V, the accumulated thermal budget in processing is much higher in the more complex detector wafer process, leading to more compensation or removal of the p-type doping. Nonetheless, the rate of this apparent acceptor removal, also denoted as β, is remarkably similar for both batches. The approximate value of 5.95×10^{8} cm^{-3} kGy $^{-1}$ is in good agreement with the literature for both p-type MCz silicon with 8×10^{8} cm^{-3} kGy $^{-1}$[34], and n-type float zone silicon with 3-8×10^{8} cm^{-3} kGy $^{-1}$[33, 37].

The compensation of space charge is indeed confirmed by red laser TCT measurements (Fig. 13). For sensors from the pixel detector wafer (Fig. 13b), the waveforms show a transition of the peak of the electric field, i.e. the p-n junction, towards the backplane of the sensor. Given that the n^{+} front and p^{+} backside implants are not changed, this is only explained by an inversion of effective bulk space charge from effective p-type (negative space charge) to n-type (positive space charge) as a consequence of gamma irradiation. Just like in C-V measurements, a similar trend is visible for the test structure diodes, but to a lesser extent (Fig. 13a), due to their higher initial doping concentration, which does not undergo SCSI in the shown dose range.

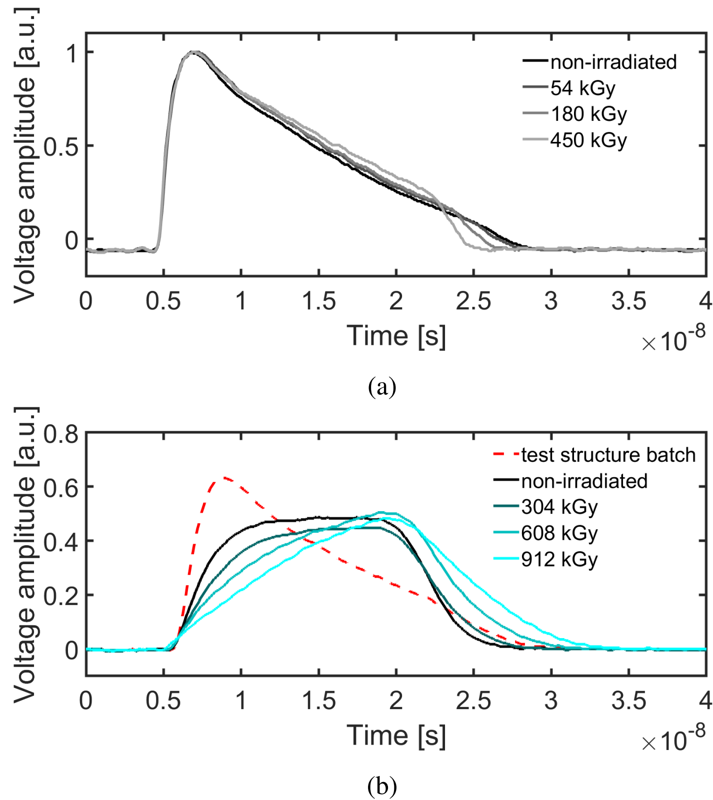

Figure 13: Change in transient signal at -150 V generated with red laser upon gamma irradiation in a) representative test structure wafer diode, b) pixel detector layout diode with H_2O + O_3 -deposited Al_2O_3. Compensation of negative space charge with gamma irradiation is observed, leading to space charge sign inversion for newer pixel detector layout diodes, in agreement with Fig. 11.

267 Signals obtained in TCT with IR laser (Figure 14a) are used to evaluate the charge collection
268 efficiency with irradiation by integrating over the entire length of the signal (Figure 14b). Gamma
269 irradiation does not significantly affect the CCE, in fact, full charge collection is simply achieved
270 earlier for diodes with low doping concentration before and after SCSI, in agreement with earlier
271 depletion shown in Figures 11 and 12. As all charge can be collected within 20-25 ns, the differences
272 in signal rise time and amplitude are not expected to affect device operation in particle tracking
273 applications where no precision timing is required.

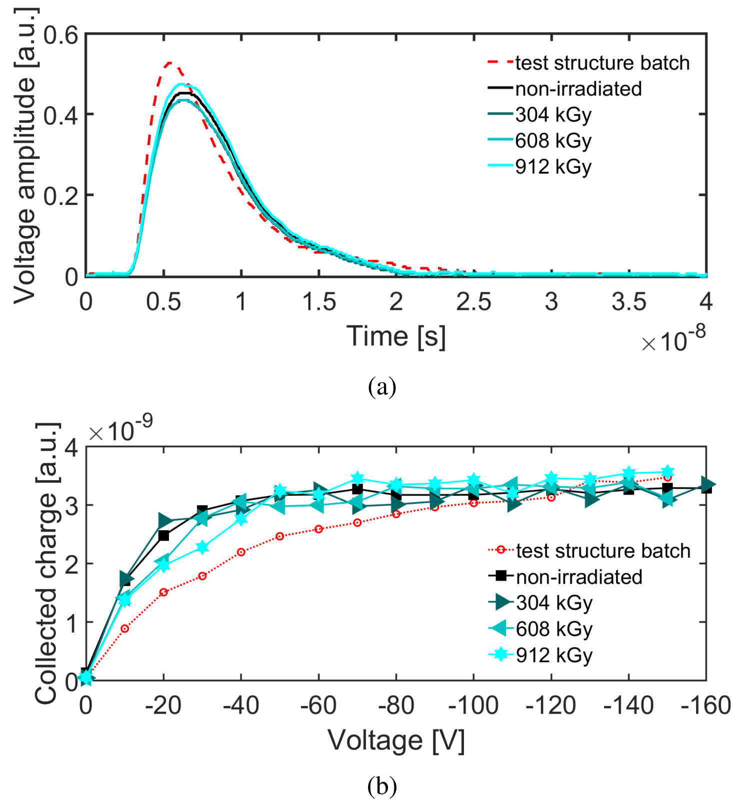

Figure 14: a) Transient signal at -150 V generated with infrared laser upon gamma irradiation in pixel detector layout diode with H_2O + O_3 -deposited Al_2O_3, b) collected charge for different gamma irradiation doses.No significant deterioration of the signal nor charge collection is observed.

The most prominent effect of gamma irradiation is observed on the charge of the Al_2O_3 films, as originally hypothesized. Figure 15 shows the MOS capacitor CV curves of different ALD oxidants with gamma radiation dose.

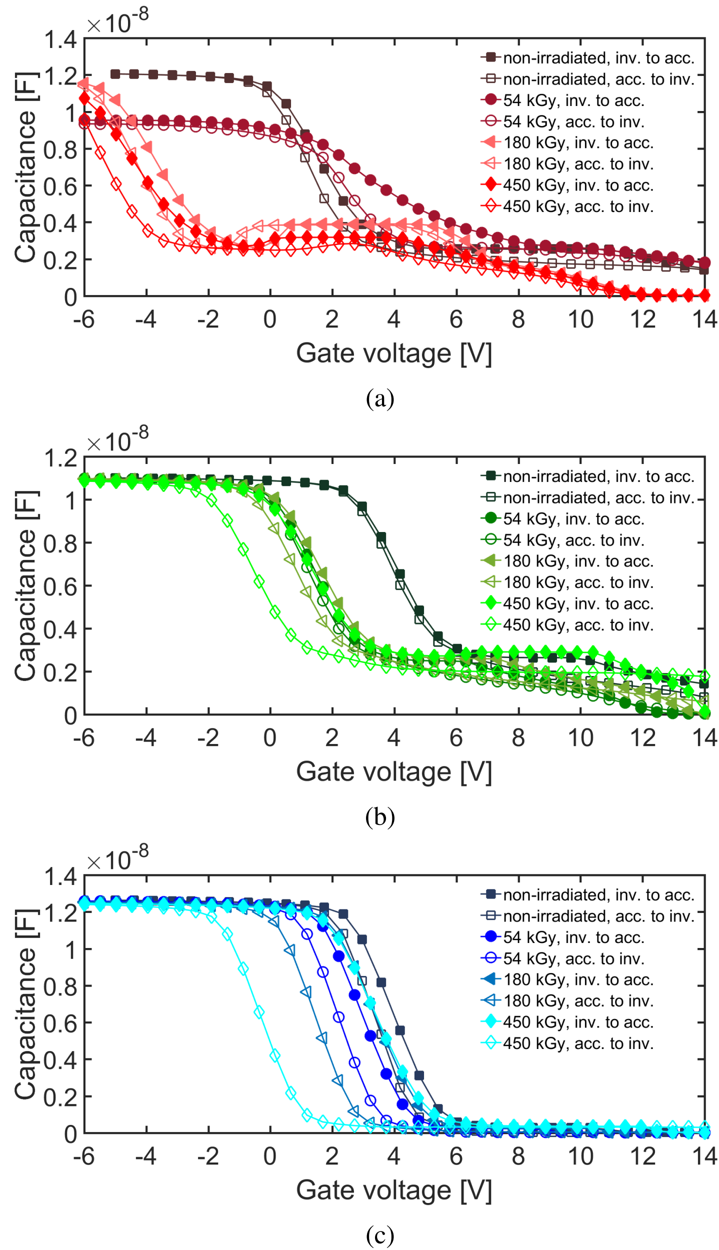

Figure 15: C-V curves for MOS capacitors with Al_2O_3 films deposited using different oxidants: a) H_2O, b) H_2O + O_3 c) O_3.

Figure 16 shows the effective charges Q_{eff} for the different oxidants, as well as for the pixel detector diodes, as a function of gamma radiation dose. The charge manifested in interface traps is referred to as mobile charge Q_m, as its appearance depends on the direction of the voltage application. For diodes from the pixel detector wafer irradiated with high gamma radiation doses, results were extracted at lower measurement frequencies of 20-100 Hz for better reliability.

For the Al_2O_3 films grown with H_2O (Figure 16a), the entire effective (fixed) charge of the film, represented by the curve recorded from inversion to accumulation, is changed from negative to positive at higher doses (the curve at 54 kGy is assumed to be an outlying sample). The hysteresis in

285 turn, which can be interpreted as charge accumulated in interface traps, increases slightly. The film
286 deposited with O_3 (Figure 16c) behaves very differently: while the fixed charge remains the same
287 under irradiation, the hysteresis of the C-V curve increases with each step in radiation dose. The
288 film deposited with a combination of H_2O and O_3 oxidants (Figure 16b) represents a compromise
289 between the individual oxidants even now: after a first partial compensation of the negative oxide
290 charge to the lowest gamma ray dose, the fixed charge remains the same, and only the hysteresis and
291 thus the number of interface trap charges are increased. The effective charge remains negative over
292 the dose range studied here.

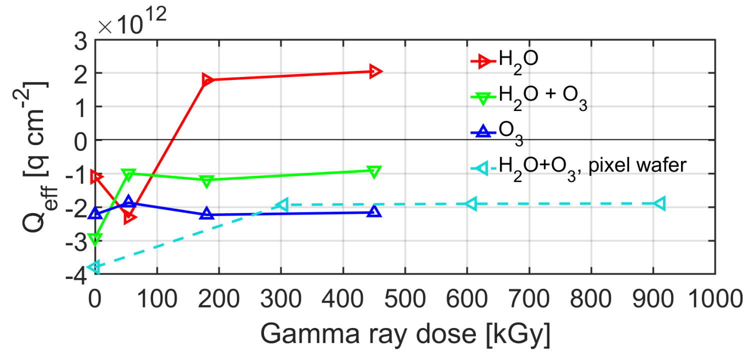

(a)

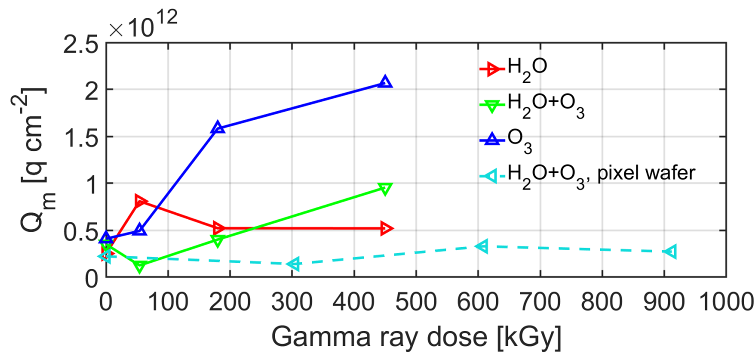

(b)

Figure 16: Evolution of effective fixed charge Q_{eff} and mobile interface trap charge Q_m in gamma-irradiated MOS capacitors for different oxidants.

293 It is notable that for films deposited with H_2O or H_2O + O_3 as oxidant, the compensation of
294 the fixed oxide charge appears to saturate after a certain dose, with almost no change observed
295 between 180 and 450 kGy. This is also well evident in Fig. 16a, which suggests stabilization of
296 the fixed charge at 180 kGy or before. On the other hand, the mobile interface charge increases
297 with radiation dose for the O_3 and H_2O + O_3 oxidants, but the increase is less for the H_2O +
298 O_3 combination. The observation of no change in oxide charge or saturation of positive charge
299 accumulation resemble earlier irradiation experiments on MOS capacitors with Al_2O_3 thin films
300 for lower doses up to 300 kGy, where little effect of irradiation on the charge was reported.[38, 39]
301 However, in these studies films deposited with H_2O were concluded as more radiation-hard, and
302 accumulation of mobile charge in form of a hysteresis was not significant. The different outcomes

303 might be explained by the thicker films used here, which are more efficient in trapping charges
304 or hydrogen that may be released from the film and the interface in irradiation. Furthermore,
305 films deposited with O_3 have been shown to trap charges more efficiently than films deposited with
306 water.[40] Our high-resistivity MCz substrates may also be more sensitive to interface traps and
307 mobile charges manifested as hysteresis of MOS capacitor C-V curves, than the substrates with
308 higher doping concentration used in [38].

309 Table 2 summarizes the most important effects of gamma irradiation on the devices. Although
310 α and β parameters are properties of the bulk, results are shown for oxidants separately to allow
311 for cross-validation between different wafers. It is again evident that films deposited with only
312 H_2O as oxidant show a positive oxide charge after irradiation, which would be detrimental for
313 surface insulation between n+ implants.

Table 2: Effect of gamma irradiation on the properties of diodes and MOS capacitors fabricated with Al_2O_3 using different ALD oxidants: leakage current damage parameter α, doping concentration compensation rate β, and maximum effective oxide charge $Q_{eff,max}$ which appears to saturate at higher doses.

Oxidant species	H_2O	O_3	H_2O + O_3	Pixel wafer, H_2O + O_3
α, area [$\times 10^{-10}$ Acm^{-3}kGy^{-1}]	-	3.04	2.37	2.80
α, volume [$\times 10^{-9}$ Acm^{-3}kGy^{-1}]	-	9.49	7.40	8.75
β [$\times 10^{8}$ cm^{-3}kGy^{-1}]	-	-	-5.98	-5.93
$Q_{eff,max}$ [$\times 10^{12}$ qcm^{-2}]	2.05	-2.16	-0.90	-1.89

314 The results obtained in this study show that a balance between the accumulation of mobile
315 charge (O_3) and fixed oxide charge (H_2O) is offered simply by combining these precursors. Irradi-
316 ation of the pixel wafer devices, which contain a film deposited by the H_2O + O_3 combination, to
317 even higher doses up to 912 kGy confirm this observation. Considering the electrical properties in
318 devices and in terms of resistance to gamma irradiation, the combination of H_2O + O_3 oxidants is
319 confirmed to provide the best properties for Al_2O_3 in silicon detectors in an environment with high
320 ionizing doses.

321 4 Summary and conclusions

322 We have shown the electrical characterization of diodes and MOS capacitors fabricated on magnetic
323 Czochralski silicon substrates. These devices contain Al_2O_3 as field insulator deposited with ALD
324 using different oxidants.

325 We observe that leakage currents in diodes before the onset of breakdown are low for all studied
326 ALD processes. Charge collection in TCT is also independent of the choice of oxygen precursor.
327 It was found that with the most common ALD process for the deposition of Al_2O_3 thin films, using
328 TMA and H_2O as oxidant, a comparably low negative oxide charge is achieved. This property is
329 related to diodes exhibiting the highest breakdown voltages compared to the other oxidants, when
330 not irradiated. However, it also manifests itself as clearly inferior resistance to gamma irradiation:
331 eventually, the oxide charge is compensated to positive, and also the stability of diode currents
332 appears to suffer during irradiation. When the abovementioned results are considered together with

the blistering of Al_2O_3 films, which is especially detrimental for finely segmented devices and is not observed for O_3 -containing ALD processes, it is concluded that the use of O_3 in ALD of Al_2O_3 for pixel detectors is a viable strategy for overcoming the weaknesses of Al_2O_3 when deposited with H_2O. Electrical characterization before and after gamma irradiation show that the addition of O_3, i.e. to employ a combination of oxidants instead of O_3 only, yields the best combination of properties. Films deposited by O_3 alone show early breakdown in diodes as a consequence of very high negative charge. Irradiation with gamma rays levels out the properties achieved by the O_3 and $H_2O + O_3$ ALD processes, therefore O_3 alone should still not be ruled out for further use in silicon detectors for challenging radiation environments.

In addition to its effect on the Al_2O_3 films, gamma irradiation was also observed to lead to a compensation of space charge, and even space charge sign inversion for lower effective doping concentrations, in the silicon bulk. This phenomenon has been reported earlier for Cz-Si.[34] This observation reminds us that the effects of ionizing radiation and the manifestation of radiation damage in p-type silicon in general are not to be neglected. This is especially the case in Cz-Si with its high oxygen content and sensitivity to thermal donors. On the other hand, it should be noted that at least at low effective doping concentrations, space charge compensation or even space charge sign inversion apparently do not negatively affect the charge collection efficiency of devices, and may even be initially beneficial by lowering the depletion voltage, as has been suggested earlier for Cz-Si.[35, 36]

Acknowledgments

J. Ott would like to thank the Vilho, Yrjö and Kalle Väisälä Foundation of the Finnish Academy of Science and Letters for financial support. S. Bharthuar, T. Naaranoja and L. Martikainen acknowledge funding from the Magnus Ehrnrooth foundation. Facilities for detector fabrication were provided by Micronova Nanofabrication Centre in Espoo, Finland within the OtaNano research infrastructure. The authors are grateful to Dr. Eija Tuominen and the Helsinki Detector Laboratory for providing the environment for electrical measurements. This study has been partially funded by the Horizon 2020 ERA Chair project, grant agreement 669014 (Particle and Radiation Detectors, Sensors and Electronics in Croatia, PaRaDeSEC).

References

[1] CMS Collaboration, "The Phase-2 Upgrade of the CMS Tracker, Technical Design Report." CERN-LHCC-2017-009CMS-TDR-0141, 2017.

[2] A. G. Aberle, S. Glunz and W. Warta, *Impact of illumination level and oxide parameters on Shockley-Read-Hall recombination at the Si-SiO2 interface*, *Journal of Applied Physics* **71** (1992) 4222.

[3] J. Schwank, M. Shaneyfelt, D. Fleetwood, J. Felix, P. Dodd, P. Paillet et al., *Radiation Effects in MOS Oxides*, *IEEE Transactions on Nuclear Science* **55** (2008) 1833.

[4] G. Pellegrini, C. Fleta, F. Campabadal, M. Miñano, M. Lozano, J. Rafí et al., *Technology of p-type microstrip detectors with radiation hard p-spray, p-stop and moderated p-spray insulations*, *Nuclear Instruments and Methods in Physics Research A* **579** (2007) 599–.

372 [5] J. Schwandt, *CMS Pixel detector development for the HL-LHC*, Nuclear Instruments and Methods in
373 Physics Research A **924** (2019) 59.

374 [6] M. Christophersen and B. F. Phlips, *Alumina, Al_2O_3, Layers as Effective P-Stops for Silicon Radiation*
375 *Detectors*, IEEE NSS Conference Record (2011) 113.

376 [7] J. Härkönen, E. Tuovinen, P. Luukka, A. Gädda, T. Mäenpää, E. Tuominen et al., *Processing of*
377 *n+/p−/p+ strip detectors with atomic layer deposition (ALD) grown Al2O3 field insulator on*
378 *magnetic Czochralski silicon (MCz-si) substrates*, Nuclear Instruments and Methods in Physics
379 Research A **828** (2016) 46.

380 [8] J. Härkönen, J. Ott, M. Mäkelä, T. Arsenovich, A. Gädda, T. Peltola et al., *Atomic Layer Deposition*
381 *(ALD) grown thin films for ultra-fine pitch pixel detectors*, Nuclear Inst. and Methods in Physics
382 Research, A **831** (2016) 2.

383 [9] G. Dingemans and W. Kessels, *Status and prospects of Al2O3-based surface passivation schemes for*
384 *silicon solar cells*, Journal of Vacuum Science and Technology A **30** (2012) 040802.

385 [10] B. Hoex, J. J. H. Gielis, M. C. M. van de Sanden and W. M. M. Kessels, *On the c-Si surface*
386 *passivation mechanism by the negative-charge- dielectric Al2O3*, Journal of Applied Physics **104**
387 (2008) 113703.

388 [11] F. Werner, B. Veith, D. Zielke, L. Kühnemund, C. Tegenkamp, M. Seibt et al., *Electronic and*
389 *chemical properties of the c-Si/Al2O3 interface*, Journal of Applied Physics **109** (2011) 113701.

390 [12] T. Suntola, *Atomic layer epitaxy*, Materials Science Reports **4** (1989) 261.

391 [13] M. Leskelä and M. Ritala, *Atomic layer deposition (ALD): from precursors to thin film structures*,
392 Thin Solid Films **409** (2002) 138.

393 [14] S. M. George, *Atomic Layer Deposition: An Overview*, Chemical Reviews **110** (2011) 111.

394 [15] P. Repo, H. Talvitie, S. Li, J. Skarp and H. Savin, *Silicon Surface Passivation by Al2O3: Effect of*
395 *ALD Reactants*, Energy Procedia **8** (2011) 681.

396 [16] G. von Gastrow, S. Li, P. Repo, Y. Bao, M. Putkonen and H. Savin, *Ozone-based batch atomic layer*
397 *deposited Al2O3 for effective surface passivation*, Energy Procedia **38** (2013) 890.

398 [17] S. Li, P. Repo, G. von Gastrow, Y. Bao and H. Savin, *Effect of ALD Reactants on Blistering of*
399 *Aluminum Oxide Films on Crystalline Silicon*, IEEE 39th Photovoltaic Specialists Conference, Tampa
400 Bay, Florida, USA (2013) 1265.

401 [18] L. Spiegel, T. Barvich, B. Betchart, S. Bhattacharya, S. Czellar, R. Demina et al., *Czochralski silicon*
402 *as a detector material for S-LHC tracker volumes*, Nuclear Instruments and Methods in Physics
403 Research A **628** (2011) 242.

404 [19] J. Härkönen, E. Tuovinen, P. Luukka, H. K. Nordlund and E. Tuominen, *Magnetic Czochralski silicon*
405 *as detector material*, Nuclear Instruments and Methods in Physics Research Section A: Accelerators,
406 Spectrometers, Detectors and Associated Equipment **579** (2007) 648.

407 [20] W. Kern and D. A. Puotinen, *Cleaning solutions based on hydrogen peroxide for use in silicon*
408 *semiconductor technology*, RCA Reviews **31** (1970) 187.

409 [21] D. Schroder, *Semiconductor Material and Device Characterization*. Wiley, 1990.

410 [22] V. Eremin and Z. Li, *Determination of the fermi-level position for nutron-irradiated high-resistivity*
411 *silicon detectors and materials using the transient charge technique (tcht)*, IEEE Transactions on
412 Nuclear science **41** (1994) 1907.

413 [23] V. Eremin, N. Strokan, E. Verbitskaya and Z. Li, *Development of transient current and charge*
414 *techniques for the measurement of effective net concentration of ionized charges (neff) in the space*
415 *charge region of p-n junction detectors*, *Nuclear Instruments and Methods in Physics Research*
416 *Section A: Accelerators, Spectrometers, Detectors and Associated Equipment* **372** (1996) 388.

417 [24] E. Fretwurst, V. Eremin, H. Feick, J. Gerhardt, Z. Li and G. Lindström, *Investigation of*
418 *damage-induced defects in silicon by TCT*, *Nuclear Instruments and Methods in Physics Research*
419 *Section A: Accelerators, Spectrometers, Detectors and Associated Equipment* **388** (1997) 356 .

420 [25] G. Kramberger, V. Cindro, I. Mandić, M. Mikuž, M. Milovanović, M. Zavrtanik et al., *Investigation of*
421 *Irradiated Silicon Detectors by Edge-TCT*, *IEEE Transactions on Nuclear Science* **57** (2010) 2294.

422 [26] S. Ramo, *Currents induced by electron motion*, *Proceedings of the IRE* **27** (1939) 584.

423 [27] W. Shockley, *Currents to Conductors Induced by a Moving Point Charge*, *Journal of Applied Physics*
424 **9** (1938) 635.

425 [28] V. Eremin, N. Fadeeva, E. Verbitskaya, D. Mitina, J. Ott, J. Härkönen et al., *Operation of voltage*
426 *terminating structure in silicon n+-p-p+ detectors with Al2O3 field isolator grown by Atomic Layer*
427 *Deposition method*, *Journal of Instrumentation* **13** (2018) P11009.

428 [29] J. Ott, A. Gädda, S. Bharthuar, E. Brücken, M. Golovleva, J. Härkönen et al., *Processing of*
429 *AC-coupled n-in-p pixel detectors on MCz silicon using atomic layer deposited aluminium oxide*,
430 *Nuclear Instruments and Methods in Physics Research Section A: Accelerators, Spectrometers,*
431 *Detectors and Associated Equipment* **958** (2020) 162547.

432 [30] J. Ott, T. P. Pasanen, A. Gädda, M. Garín, K. Rosta, V. Vähänissi et al., *Impact of doping and silicon*
433 *substrate resistivity on the blistering of atomic-layer-deposited aluminium oxide*, *Applied Surface*
434 *Science* **522** (2020) 146400.

435 [31] E. Fretwurst, G. Lindström, J. Stahl, I. Pintilie, Z. Li, J. Kierstead et al., *Bulk damage effects in*
436 *standard and oxygen-enriched silicon detectors induced by 60Co-gamma radiation*, *Nuclear*
437 *Instruments and Methods in Physics Research A* **514** (2003) 1.

438 [32] I. Pintilie, E. Fretwurst, G. Lindström and J. Stahl, *Results on defects induced by 60Co gamma*
439 *irradiation in standard and oxygen-enriched silicon*, *Nuclear Instruments and Methods in Physics*
440 *Research A* **514** (2003) 18.

441 [33] Z. Li, E. Verbitskaya, E. Fretwurst, J. Kierstead, V. Eremin, I. Ilyashenko et al., *Paradoxes of*
442 *steady-state and pulse operational mode characteristics of silicon detectors irradiated by ultra-high*
443 *doses of* γ*-rays*, *Nuclear Instruments and Methods in Physics Research A"* **514** (2003) 25.

444 [34] Z. Li, M. Bruzzi, V. Eremin, J. Härkönen, J. Kierstead, P. Luukka et al., *Gamma radiation induced*
445 *space charge sign inversion and re-inversion in p-type mcz si detectors and in proton-irradiated*
446 *n-type mcz si detectors*, *Nuclear Instruments and Methods in Physics Research Section A:*
447 *Accelerators, Spectrometers, Detectors and Associated Equipment* **552** (2005) 34.

448 [35] J. Härkönen, E. Tuovinen, P. Luukka, E. Tuominen and Z. Li, *p+/n-/n+ cz-si detectors processed on*
449 *p-type boron-doped substrates with thermal donor induced space charge sign inversion*, *IEEE*
450 *Transactions on Nuclear Science* **52** (2005) 1865.

451 [36] E. Tuovinen, J. Härkönen, P. Luukka and E. Tuominen, *Intentional thermal donor activation in*
452 *magnetic czochralski silicon*, *Materials Science in Semiconductor Processing* **10** (2007) 179.

453 [37] Z. Li, J. Härkönen, W. Chen, J. Kierstead, P. Luukka, E. Tuominen et al., *Radiation hardness of high*
454 *resistivity magnetic Czochralski silicon detectors after gamma, neutron, and proton radiations*, *IEEE*
455 *Transactions on Nuclear Science* **51** (2004) 1901.

456 [38] J. Rafí, G. Pellegrini, V. Fadeyev, Z. Galloway, H.-W. Sadrozinski, M. Christophersen et al., *Gamma and proton irradiation effects and thermal stability of electrical characteristics of metal-oxide-silicon capacitors with atomic layer deposited Al2O3 dielectric*, *Solid-State Electronics* **116** (2016) 38.

459 [39] A. Suria, H. C. Chiamori, A. Shankar and D. G. Senesky, *Capacitance-voltage characteristics of gamma irradiated Al2O3, HfO2, and SiO2 thin films grown by plasma-enhanced atomic layer deposition*, *Proceecings of SPIE* **9491** (2015) 949105.

462 [40] M. B. González, J. M. Rafí, O. Beldarrain, M. Zabala and F. Campabadal, *Charge trapping analysis of Al2O3 films deposited by atomic layer deposition using H2O or O3 as oxidant*, *Journal of Vacuum Science and Technology B* **31** (2013) 01A101.